Available online at www.sciencedirect.com

SciVerse ScienceDirect

Scripta Materialia 69 (2013) 171–174

Scripta MATERIALIA

www.elsevier.com/locate/scriptamat

Electrostatic assembly of mesoporous $Li_4Ti_5O_{12}$/graphene hybrid as high-rate anode materials

Shuping Pang,[a,1] Yunyan Zhao,[a,b,1] Chuanjian Zhang,[a] Qinghua Zhang,[c] Lin Gu,[c] Xinhong Zhou,[b] Guicun Li[b,*] and Guanglei Cui[a,*]

[a] *Qingdao Key Lab of Solar Energy Utilization and Energy Storage Technology, Qingdao Institute of Bioenergy and Bioprocess Technology, Chinese Academy of Sciences, Qingdao 266101, PR China*

[b] *Qingdao University of Science and Technology, Qingdao 266042, PR China*

[c] *Beijing National Laboratory for Condensed Matter Physics, The Institute of Physics, Chinese Academy of Sciences, Beijing 100190, PR China*

Received 16 January 2013; accepted 25 February 2013
Available online 24 March 2013

Mesoporous $Li_4Ti_5O_{12}$/graphene hybrid was synthesized by an electrostatic assembly method to serve as the high rate anode material for lithium batteries. The graphene sheets were strongly attatched with $Li_4Ti_5O_{12}$ spheres and thus can form an efficient electrically conducting network permeating in the electrode to speed the charge and discharge process. The discharge capacity of $Li_4Ti_5O_{12}$/graphene hybrid was improved to 124 mAh g^{-1} at 20 C-rate, which is more than twice the value of the $Li_4Ti_5O_{12}$ electrode.

Keywords: Nanocomposite; Self-assembly; Electrochemistry; Anode material; Lithium-ion batteries

High power lithium ion batteries (LIBs) is the essential part of electric vehicle (EV) and hybrid electric vehicle (HEV) to fulfill the ultra-fast charging [1,2]. As a zero-strain insertion material, spinel $Li_4Ti_5O_{12}$ (LTO) is considered as one of the most promising anode for the EV and HEV due to its outstanding reversibility, long lifetime and eminent safety [3–5]. Nevertheless its rate performance is strongly limited by the inherent low electrical conductivity (ca. 10^{-13} S cm^{-1}) [6,7]. In this regard, conductive component such as carbon, silver and tin have been devoted to resolve this problem by making a composite [8–12].

Among these conductive materials, graphene is more competitive than others owing to its high pristine conductivity and the two dimensional (2D) structure characteristic [13–16]. Nanosized LTO structures, such as nanosheets and nanoparticles have been in situ synthesized on the surface of graphene to construct nano-hybrid materials, resulting in an excellent rate performance and cycle stability [17–19]. Whereas, the nanosized material has a low volumetric density and thus fails to meet the requirement of high powder tap density and volumetric energy density of the cell [20,21].

Motivated by this, herein, a facile electrostatic adsorption method was employed to synthesize mesoporous LTO/graphene hybrid [22–24]. Mesoporous LTO spheres were firstly treated with HNO_3 to form a negative charged surface and then poly(ethylene imine) was employed to join the LTO particles and the graphene oxide (GO) sheets together. The strong electrostatic adsorption and the 2D morphology of the graphene sheets render the hybrid material an improved rate performance. The discharge capacity reaches 138 $mAhg^{-1}$ at 10 C-rate. Most importantly, such electrostatic adsorption method is potentially extendable to many other lithium ion battery materials.

All reagents were used as received without further purification. The mesoporous TiO_2 spheres were prepared as reported by Zhong and co-workers [25]. Firstly, 6 mL butyl titanate was dissolved in 150 mL ethylene glycol and stirred for eight hours. Then the solution was poured into a 520 mL mixed solution which contained acetone and deionized water with a volume ratio of 340:1. Secondly, the obtained white precursor was

* Corresponding authors. Tel.: +86 532 80662746; fax: +86 532 80662744 (G. Cui); e-mail: cuigl@qibebt.ac.cn

[1] These authors contributed to the work equally.

1359-6462/$ - see front matter
http://dx.doi.org/10.1016/j.scriptamat.2013.02.049

refluxed with water at 100 °C for 2 h to form the mesoporous TiO_2 spheres. The precipitate was separated by centrifugation and washed with deionized water and ethyl alcohol for several times and then dried at 60 °C for 3 h. 0.500 g mesoporous TiO_2, 0.595 g lithium acetate dihydrate and 0.115 g polyethylene glycol 20000 (PEG 20000) as a carbon source were mixed in 20 ml alcohol and stirred at 70 °C for 1 h, followed by drying overnight at 80 °C. Then, this mixture was annealed at 800 °C for 20 h under N_2 atmosphere to gain carbon-coated mesoporous LTO spheres (LTO-C). For the synthesis of graphene bridge connected mesoporous LTO (LTO-G), in the first step, 0.360 g above-described LTO-C spheres were treated with HNO_3 (5%) for 2 h. After repeatedly washed with distilled water, the LTO-C nanoparticles were modified by 50.00 ml poly(ethylene imine) (PEI) (0.2 wt%) to render their surface positively charged. In the second step, graphene oxide (GO) was prepared by a modified Hummers method from purified natural graphite powder [26]. 35 mg GO was dispersed into 50.00 mL distilled water, followed by the addition of positively charged nanoparticles with stirring. The sample was then dried in an oven at 60 °C, and finally heat treated at 400 °C in N_2 for 2 h to obtain LTO-G nanohybrid.

The phase composition of the samples was characterized using X-ray diffraction (XRD, Bruker-AXS Microdiffractometer D8 ADVANCE) with Cu Ka radiation ($\lambda = 1.5406$ Å) from 10° to 80°. The morphology of the synthesized materials was observed using a field-emission scanning electron microscopy (FESEM, HITACHI S-4800) and a transmission electron microscope (TEM, JEOL 2100F). The high-resolution transmission electron microscopy (HR-TEM) image was carried out on a JEOL JEM-2010 (HR) electron microscope operated at 200 kV. The content of coated carbon in $Li_4Ti_5O_{12}$ sample was determined by thermogravimetry (TG) analysis with a Rubotherm-DYNTHERM-HP instruments.

Electrochemical experiments were carried out using standard R2032 type coin cells assembled in an argon-filled glove box. The anodes were prepared by mixing 80 wt% active material, 10 wt% conductive carbon black and 10 wt% poly(vinyl difluoride) (PVDF) with appropriate amount of N-methyl-2-pyrrolidone solvent. The slurry was cast on Cu foil to a thickness of approximately 70 μm and subsequently dried in a vacuum oven at 120 °C for 8 h to remove the residual solvent. Pure lithium foil was used as the counter electrode and separated by a Celgard 2500 membrane separator. The electrolyte solution was 1 M $LiPF_6$ in ethylene carbonate/dimethyl carbonate (1:1 by volume). Galvanostatical discharge-charge experiments were conducted over a voltage range of 1.0–3.0 V (vs Li^+/Li) at different rates using a LAND battery testing system. Electrochemical impedance spectroscopy (EIS) measurements were carried out on a ZAHNER ZENNIUM electrochemical workstation by applying a sine wave with an amplitude of 5.0 mV over the frequency range from 100 kHz to 100 mHz.

The fabrication process of the LTO-G nano-hybrid is illustrated in Scheme 1. LTO-C spheres were firstly treated in HNO_3 solution and then immersed in 0.2% PEI solution to render the surface of LTO-C spheres more positive, named as modified LTO. Whereas, GO sheets present a negative charge originated from the ionization of the carboxylic acid and phenolic hydroxy groups on their surface [23]. Adding the positively charged LTO-C spheres into the dilute GO solution can acquire the uniform assembly of LTO-C spheres on GO sheets by the electrostatic interaction [27]. Finally, the GO sheets were thermally reduced to electrical conductive graphene to serve as an electron transfer pathway in the hybrid material [28,29].

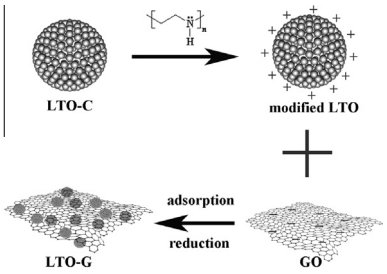

Scheme 1. Schematic illustration of the electrostatic assembly of LTO-G.

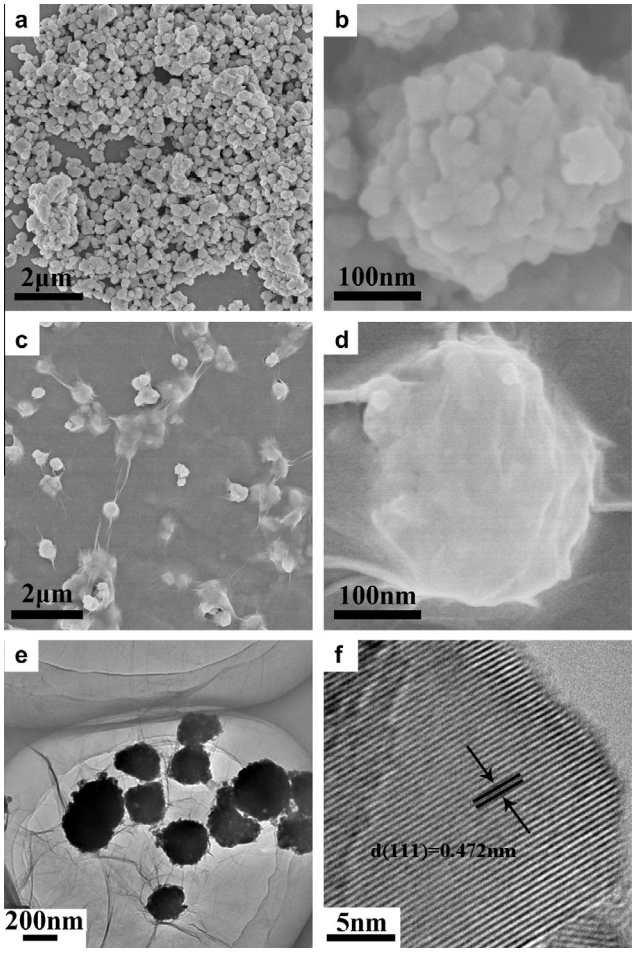

Figure 1. Typical SEM images of (a and b) LTO-C and (c and d) LTO-G, (e) Typical TEM image of LTO-G, (f) Typical HRTEM image of LTO-G.

Figure 1a and b display the as-prepared mesoporous LTO-C spheres, gained by a solid state reaction between mesporous TiO_2 (SEM image of TiO_2 can be seen in supporting information Fig. S1) and lithium acetate dihydrate in the presence of PEG 20000. The LTO-C mesoporous spheres are monodispersed in the range of 300–500 nm as shown in Figure 1a. The magnified SEM image in Figure 1b reveals that the mesoporous spheres are assembled with 10–20 nm primary nanoparticles. The formation of the mesoporous sturcture of LTO-C is benefited from the presence of PEG 20000, which can be carbonized at high temperature and efficiently restrict the growth of primary particles [21]. After the electrostatic assembly of LTO-C with GO and followed by the thermal reduction, LTO-G nanohybrid was formed as shown in Figure 1c and d. The LTO-C spheres uniformly attached and embeded onto the graphene sheets. The amount of GO we used in the hybrid material is ~10%. On calcination in 400 °C in N_2 for 2 h, the GO sheets are reduced to graphene and the content of graphene was calculated to be ~5% (see TG curve in Fig. S2). It is proposed that such hybrid structure is in favor of the realization of fast transport the electrons in the electrode. TEM image of LTO-G (Fig. 1e) shows clearly that LTO-C spheres are bridged by graphene sheets. The HRTEM image in Figure 1f shows the highly crystallized LTO nanoparticle. A distance of the clear lattice fringe is 0.472 nm, which is consistent with the (1 1 1) atomic planes of the spinel LTO. XRD patterns of LTO-G in supporting information Figure S3 demonstrates that LTO crystals in the LTO-G composites are well maintained in the nitric acid treatment and electrostatic assembly processes. It can be seen from Figure 1f that the surface of primary particles was surrounded by a thin uniform carbon coating layer, derived from the decomposition and carbonization of the organic PEG precursor during the solid state reaction [21]. In the hybrid material, carbon coating layer links every primary particle into a submicrosphere, and every submicrosphere is further bridged by 2D graphene sheets. Therefore, the hybrid structure is rational to possess an excellent electrical property due to the successful construction of the 3 D conducting network in the hybrid material [30].

The galvanostatic charge and discharge voltage profiles and specific capacities of LTO-C and LTO-G samples were tested at different rates within the potential window of 1–3 V as shown in Figure 2. At different current rates of 0.1 C, 1 C, 5 C, 10 C and 20 C, the LTO-C presents reversible capacities of 173, 107, 70, 52 and 40 $mAhg^{-1}$, respectively (Fig. 2a), while after the subsequent introduction of graphene bridge, those capacities increase to 180, 165, 154, 140 and 124 $mAhg^{-1}$ as shown in Figure 2b (1 C means insertion of 3 mol Li into $Li_4Ti_5O_{12}$ in 1 h). It can be also seen clearly that the polarization for the LTO-G sample is significantly lower compared to the LTO-C sample, especially at high current rates. Figure 2c compares the rate capabilities of LTO-C and LTO-G in a range of discharge rate from 0.1 C to 20 C. At a low current rate of 0.1 C, the capacities of LTO-G are slightly higher than those of LTO-C due to the contribution of graphene. Whereas, the capacities of LTO-G at high current rates are much

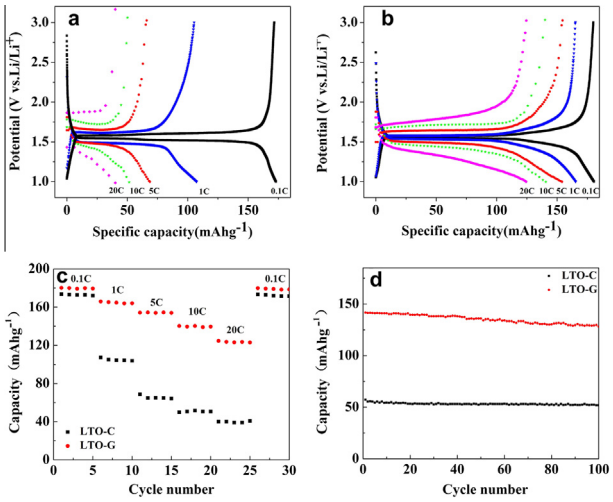

Figure 2. (a) The discharge/charge curves of LTO-C at 0.1 C, 1 C, 5 C, 10 C and 20 C; (b) The discharge/charge curves of LTO-G at 0.1 C, 1 C, 5 C, 10 C and 20 C; (c) Cycling performance of LTO-C and LTO-G at different rates; (d) Cycling performance of LTO-C and LTO-G at 10 C.

higher than those of LTO-C, particularly the capacities of LTO-G are twice higher than that of LTO-C at 20 C. The cyclabilities of LTO-C and LTO-G at 10C are shown in Figure 2d. The initial capacity of LTO-G reaches 141 mAh g^{-1} at 10 C, which slightly decreases to 129 mAh g^{-1} after 100 cycles with a capacity loss of 9%. However, for the LTO-C sample, the initial capacity at 10 C is only 77 mAh g^{-1} and decreases to 62 mAh g^{-1} after 100 cycles.

To deeply understanding the contribution of graphene sheets on electrochemistry performance, the EIS measurements were performed (Fig. 3). The depressed semicircles in high-middle frequency are associated with the charge transfer resistance (Rct). The Rct value of LTO-G sample (230 Ω) is significantly lower than that of LTO-C (450 Ω), the decrease of Rct is beneficial to the transportation of lithium ions and electrons. The improvement of the electrochemical performance is ascribed to the high electrical conductivity and the unique 2D structure of the graphene sheets. The graphene in the hybrid electrode can effectively link the active LTO spheres and the current collector, which endow the hybrid material the outstanding cycling stability and

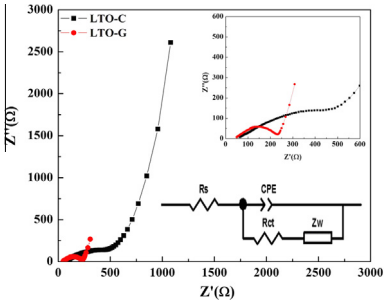

Figure 3. Nyquist plots for LTO-C and LTO-G samples, as well as the equivalent circuit used to fit the EIS. The topright inset is the enlarged Nyquist plot.

superior rate capability. Most importantly, it worth to note that the electrostatic absorption method employed in this work is a post treatment process and is easy to scale up and potentially extendable to arbitary battery materials.

In conclusion, mesoporous $Li_4Ti_5O_{12}$ bridged by graphene sheets was prepared by a facile electrostatic adsorption method. The as-obtained LTO-G nano-hybrid exhibits high reversible capacity and outstanding rate performance owing to the synergy of the good conductivity, large surface area, flexibility of graphene and good stability of mesoporous $Li_4Ti_5O_{12}$. Such electrostatic adsorption method is easy to scale up and will provide a new pathway for the production of various high rate lithium ion battery materials.

We appreciate the support of the "100 Talents" program of Chinese Academy of Sciences, National Program on Key Basic Research Project of China (973 Program) (No. MOST2011CB935700), the National Natural Science Foundation (Grant Nos. 21271180, 21275151 and 51272113) and the Qingdao Key Lab of solar energy utilization and energy storage technology.

Supplementary data associated with this article can be found, in the online version, at http://dx.doi.org/10.1016/j.scriptamat.2013.02.049.

[1] B. Kang, G. Ceder, Nature 458 (2009) 190–193.
[2] N.-S. Choi, Z. Chen, S.A. Freunberger, X. Ji, Y.-K. Sun, K. Amine, G. Yushin, L.F. Nazar, J. Cho, P.G. Bruce, Angew. Chem. Int. Ed. 51 (2012) 9994–10024.
[3] G.-N. Zhu, Y.-G. Wang, Y.-Y. Xia, Energy Environ. Sci. 5 (2012) 6652–6667.
[4] L. Shen, C. Yuan, H. Luo, X. Zhang, K. Xu, F. Zhang, J. Mater. Chem. 21 (2011) 761–767.
[5] L.F. Shen, C.Z. Yuan, H.J. Luo, X.G. Zhang, L. Chen, H.S. Li, J. Mater. Chem. 21 (2011) 14414–14416.
[6] Y.Q. Wang, L. Guo, Y.G. Guo, H. Li, X.Q. He, S. Tsukimoto, Y. Ikuhara, L.J. Wan, J. Am. Chem. Soc. 134 (2012) 7874–7879.
[7] M. Wagemaker, E.R.H. van Eck, A.P.M. Kentgens, F.M. Mulder, J. Phys. Chem. B. 113 (2008) 224–230.
[8] H. Li, H. Zhou, Chem. Commun. 48 (2012) 1201–1217.
[9] X. Guo, C. Wang, M. Chen, J. Wang, J. Zheng, J. Power Sources 214 (2012) 107–112.
[10] Z.Y. Wen, X.L. Yang, S.Y. Huang, J. Power Sources 174 (2007) 1041–1045.
[11] S. Huang, Z. Wen, J. Zhang, X. Yang, Electrochim. Acta 52 (2007) 3704–3708.
[12] R. Cai, X. Yu, X.Q. Liu, Z.P. Shao, J. Power Sources 195 (2010) 8244–8250.
[13] S. Pang, S. Yang, X. Feng, K. Müllen, Adv. Mater. 24 (2012) 1566–1570.
[14] S. Pang, Y. Hernandez, X. Feng, K. Müllen, Adv. Mater. 23 (2011) 2779–2795.
[15] S. Yang, X. Feng, L. Zhi, Q. Cao, J. Maier, K. Müllen, Adv. Mater. 22 (2010) 838–842.
[16] S. Yang, X. Feng, L. Wang, K. Tang, J. Maier, K. Müllen, Angew. Chem. Int. Ed. 49 (2010) 4795–4799.
[17] Y. Tang, F. Huang, W. Zhao, Z. Liu, D. Wan, J. Mater. Chem. 22 (2012) 11257–11260.
[18] H.-K. Kim, S.-M. Bak, K.-B. Kim, Electrochem. Commun. 12 (2010) 1768–1771.
[19] L.F. Shen, C.Z. Yuan, H.J. Luo, X.G. Zhang, S.D. Yang, X.J. Lu, Nanoscale 3 (2011) 572–574.
[20] G.-N. Zhu, H.-J. Liu, J.-H. Zhuang, C.-X. Wang, Y.-G. Wang, Y.-Y. Xia, Energy Environ. Sci. 4 (2011) 4016–4022.
[21] H.-G. Jung, S.-T. Myung, C.S. Yoon, S.-B. Son, K.H. Oh, K. Amine, B. Scrosati, Y.-K. Sun, Energy Environ. Sci. 4 (2011) 1345–1351.
[22] S. Yang, X. Feng, S. Ivanovici, K. Müllen, Angew. Chem. Int. Ed. 49 (2010) 8408–8411.
[23] X. Zhou, Y.-X. Yin, L.-J. Wan, Y.-G. Guo, Adv. Energy Mater. 2 (2012) 1086–1090.
[24] G. Decher, Science 277 (1997) 1232–1237.
[25] L.-S. Zhong, J.-S. Hu, L.-J. Wan, W.-G. Song, Chem. Commun. (2008) 1184–1186.
[26] W.S. Hummers, R.E. Offeman, J. Am. Chem. Soc. 80 (1958) 1339.
[27] H. Li, S. Pang, S. Wu, X. Feng, K. Müllen, C. Bubeck, J. Am. Chem. Soc. 133 (2011) 9423–9429.
[28] D.-J. Xue, S. Xin, Y. Yan, K.-C. Jiang, Y.-X. Yin, Y.-G. Guo, L.-J. Wan, J. Am. Chem. Soc. 134 (2012) 2512–2515.
[29] X. Zhou, Y.-X. Yin, L.-J. Wan, Y.-G. Guo, Chem. Commun. 48 (2012) 2198–2200.
[30] X. Zhou, Y.-X. Yin, A.-M. Cao, L.-J. Wan, Y.-G. Guo, ACS Appl. Mater. Interf. 4 (2012) 2824–2828.